Climate Dynamics (1998) 14:489–502

G. van der Schrier · L. R. M. Maas

Chaos in a simple model of the three-dimensional, salt-dominated ocean circulation

Received: 16 July 1996 / Accepted: 29 December 1997

Abstract A simple moments model used in studying the large-scale thermally driven ocean circulation, in one hemisphere, is extended with a set of evolution equations for the basin-averaged salinity gradients. Natural formulations of the boundary conditions for the heat flux and the (virtual) salt flux are given, the latter based on the SST-evaporation feedback. Stommel's box model result, a coexisting thermal and saline solution, is retrieved in the limit of no rotation. Including rotation in a salt-dominated setting, a steady circulation is found which bifurcates for higher Rayleigh numbers in a periodic solution which becomes chaotic through a cascade of subharmonic bifurcations. Periodic motion results from two different mechanisms. First, the stable stationary state bifurcates into a periodic solution where anomalously saline water is advected by the overturning circulation. Second, this periodic solution bifurcates into a state which is dominated, during the larger part of the cycle, by diffusion and inertia, characterized by a decreasing overturning rate, and, during the subsequent shorter part of the cycle, by rapid advection and restratification of the entire basin. The basin-averaged vertical density field is stably stratified in the steady and the periodic regimes and remains statically stable in the chaotic regime.

1 Introduction

The present-day thermohaline circulation in the Atlantic extends from pole-to-pole, with characteristic sinking at high latitudes. However, this may not have always been the case as can be concluded from observed variations in the stable oxygen isotope ^{18}O content of ice-cores (Oeschger et al. 1984; Dansgaard et al. 1993). Broecker et al. (1985) suggested that these variations were characterized by the alternating presence and absence of significant North Atlantic Deep Water (NADW) formation. An increasing amount of attention is given to the possibility of the existence of other stable modes of the thermohaline circulation and to its variability, on time scales ranging from decades to millennia. Variability of the thermohaline circulation, on time scales ranging from 50–400 years, was found by Stocker and Mysak (1992) in high resolution data records. They further speculated, based on modelling results, that such variability may be due to internal dynamics of the ocean.

The existence of multiple equilibria of the thermohaline circulation first observed in box models (like Stommel's 1961 model), has also been demonstrated in 2-D models (Thual and McWilliams 1992; Quon and Ghil 1992; Cessi and Young 1992) and in 3-D ocean GCMs (Bryan 1986; Marotzke and Willebrand 1991; Weaver and Sarachik 1991). Decadal to centennial variability of the thermohaline circulation has been frequently encountered in various 2-D and 3-D ocean models (Mikolajewicz and Maier-Reimer 1990; Weaver and Sarachik 1991; Stocker and Mysak 1992; Weaver et al. 1993; Quon and Ghil 1995), while also chaotic regimes have sometimes been identified (Weaver et al. 1993; Huang and Chou 1994).

The merit of box models (Stommel 1961; Thual and McWilliams 1992; Huang and Stommel 1992) and simple models in general (Källén and Huang 1987; Quon and Ghil 1992; Cessi and Young 1992) is that they allow an analysis of physical processes which play a role in thermohaline ocean circulation in an easy and conceptually clear way. These models are therefore extremely useful when it comes to understanding more complicated model results. Parameter space can be explored with a small computational effort. Both

G. van der Schrier (✉) · L. R. M. Maas
Netherlands Institute for Sea Research, PO Box 59,
1790 AB Texel, The Netherlands
E-mail: schrier@nioz.nl

stationary and periodic solutions can be followed through parameter space. However, neither box models nor other simple analytical models (Källén and Huang 1987; Cessi and Young 1992) have incorporated the Coriolis force in their description, while Earth's rotation might provide a mechanism by which the occurrence of limit cycles, needed to describe the observed decadal to millennial variability, can be explained. In Maas (1994) (M94 hereafter) an alternative model of comparable simplicity which *does* include rotation (and wind forcing) was derived by a projection of the Navier-Stokes equations, where the inertia, associated with the rotational coupling of the circulation in the zonal and meridional planes, is being dealt with. In this model, a set of coupled nonlinear equations is obtained, describing the evolution of two vectors characterizing the state of a rectangular ocean on an f-plane. These state vectors represent the basin-averaged density gradient (related to the position of the centre of mass) and the overall angular momentum vector of the ocean.

For methodological reasons, only the evolution of the temperature field and its effect on the ocean dynamics is modelled in M94. Therefore, salinity plays no active role in determining the density of the water in that model. The present study is aimed at rectifying this deficiency by considering separate evolution equations for temperature and salinity fields, supplemented with a linear equation of state. M94's study of a purely thermal ocean is here complemented by investigating the dynamics of a salt-dominated ocean. Together these studies will form a basis for further research where temperature and salinity will be of comparable magnitude.

In virtually every model of the thermohaline circulation it is the 'mixed boundary conditions' that give rise to multiple equilibria (Marotzke 1994). Mixed boundary conditions refer to restoring temperature to a specified profile (often on a fast time scale) and specifying a salt flux, both often representing present-day climate. These boundary conditions, however, will not be applied here because restoring to climatic fields is like starting at the wrong end. The 'climatic mean' is what we want the model to produce, rather than the reverse. This brings us to reformulate the boundary conditions in the following way.

The feedback mechanisms in ocean dynamics and between ocean and atmosphere which affect the thermohaline circulation have to be taken into account in the formulation of boundary conditions. Marotzke (1994) discusses some of the major feedbacks. The first (1) is a positive feedback between an enhanced overturning circulation transporting more salt northwards and a reinforcing of the overturning through increased deep water formation. The second (2) is a negative feedback: increased northward heat transport, decreases the formation of deep water. The third feedback (3), not generally incorporated in simplified climate models (Marotzke 1994), describes the effect of increased evaporation due to northward transport of relatively warm water, which increases high-latitude salinity. If the water vapour does not rain out at the same place, this feedback produces a net effect. Warren (1983) states that this loop is an amplifying feedback and that, in the North Atlantic, the effect of higher evaporation on density due to increased sea surface temperature (SST) outweighs the direct and opposite effect that the increased SST has on density. These feedbacks, discussed here for a thermally driven circulation, of course also exist in a reversed or haline driven circulation. A stability analysis of the thermohaline circulation cannot be adequately performed in models with mixed boundary conditions since they suppress two of these feedbacks in the ocean-atmosphere system (Marotzke 1994; Nakamura et al. 1994), namely feedbacks (2) and (3). For this reason, the boundary condition for the temperature field is here formulated in terms of a specified heat flux, while the boundary condition for the salinity field is coupled via a parametrization of evaporation to the sea surface temperature.

With this coupling, only the simplest possible way of representing the SST-evaporation feedback is incorporated. We have not constructed an explicit model of water vapour transport as Nakamura et al. (1994) do, excluding the possibility of a feedback (4) between thermohaline circulation and atmospheric dynamics. The only assumption which is made in this study regarding transport of moisture through the atmosphere is that precipitation is assumed to be uniformly distributed over the basin and that excess evaporation in some areas is balanced by decreased evaporation in other areas; a simple description of the 'atmospheric' part of the hydrological cycle. The boundary conditions, include the first two feedbacks and the third in a rudimentary way such that the dynamics are not further complicated by the inclusion of an active atmosphere.

The relevance of the sea surface temperature-evaporation feedback for the thermohaline circulation was recently questioned by Hughes and Weaver (1996). They argued that '… the evolution (of the evaporation) is similar between parallel experiments with SST-dependent evaporation and under fixed fluxes.' The model-runs underlying this conclusion were performed under the traditional restoring boundary conditions on temperature, where SST is restored to zonally averaged surface data on a fast time scale. Although this latter boundary condition is very popular, it is probably not the best choice if it is used in conjunction with a SST-dependent salt flux. Apart from the earlier mentioned fact that a restoring law on temperature requires a climatological equilibrium field, the typical lifetime of SST anomalies in the North-Pacific is six months (Frankignoul and Hasselman, 1977). Relaxing the temperature field on a much faster time scale (e.g. days) underestimates the variability of SST (Mikolajewicz and Maier-Reimer 1994) and therefore the variability of

the fresh water flux. Restoring SST to a prescribed temperature field on such a fast time scale enforces more or less the spatial structure of the evaporation field. The inadequacy of a restoring law on temperature has been noted earlier (Seager et al. 1995). They state that 'such surface heat flux parametrizations effectively exclude the possibility of SST playing an active role in the thermohaline circulation', something which we wish to restore by our present choice of boundary conditions.

The paper is organized as follows: the evolution equations for angular momentum, temperature and salinity are given in Sect. 2. In Sect. 3 the boundary conditions for the temperature and salinity field are formulated. The results for a salt-dominated ocean are discussed in Sect. 4 and the study is concluded in Sect. 5.

2 Model equations

2.1 Evolution of angular momentum

An idealized rectangular and constant depth ocean basin is considered with horizontal and vertical scales W and H respectively. The rigid lid approximation is employed, so that the volume and other size related geometrical factors characterizing the basin are fixed. The motion is described by the Navier-Stokes equations in Boussinesq approximation on an f-plane. The origin of the Cartesian coordinate system, $\mathbf{x}$, is chosen in the geometric centre of the basin.

The lowest moment of the momentum field is, in an enclosed ocean, given by the basin-averaged angular momentum vector, which is defined as

$$\mathbf{L} = (\mathrm{L}_1, \mathrm{L}_2, \mathrm{L}_3) \equiv \frac{1}{\mathrm{V}} \int \mathbf{x} \times \mathbf{u} \mathrm{dV}$$

where V is the volume of the basin, dV a volume increment and $\mathbf{u}$ the velocity vector.

The density ρ is a scaled perturbation quantity

$$\rho = \frac{\rho_* - \rho_0}{\delta\rho}$$

where $\delta\rho$ denotes the scale of the density perturbations, which will be made more explicit later, while temperature T and salinity S scales naturally follow

$$T = \frac{\alpha(T_* - T_0)}{\delta\rho} \text{ and } S = \frac{\beta(S_* - S_0)}{\delta\rho} \tag{1}$$

Here α and β are the thermal and haline expansion coefficients respectively, so that, in linear approximation, $\rho = -T + S$. Asterisked quantities are original quantities while subscripts zero refer to fixed reference quantities.

The equations for the evolution of the angular momentum can be formulated along the lines set out in M94. The effect of the salinity field comes in at the evaluation of the buoyancy torque. The latter can be evaluated by employing a 'global' Taylor expansion which results in

$$\rho = x\bar{\rho}_x(t) + y\bar{\rho}_y(t) + z\bar{\rho}_z(t) + h.o.t., \tag{2}$$

where

$$\bar{\rho}_x(t) = \frac{\int_V x\rho dV}{\int_V x^2 dV}, \qquad \bar{\rho}_y(t) = \frac{\int_V y\rho dV}{\int_V y^2 dV}, \qquad \bar{\rho}_z(t) = \frac{\int_V z\rho dV}{\int_V z^2 dV}, \tag{3}$$

which are related to the coordinates of the centre of mass. This approximation of the density field results in a parallel distribution of isothermal and isohaline planes.

Summarizing, the evolution of the angular momentum vector is given by:

$$\frac{d}{dt}\mathbf{L} + \frac{f}{2}\mathbf{k} \times \mathbf{L} = \frac{g'H^2}{12}\{-\bar{\rho}_y\mathbf{i} + \bar{\rho}_x\mathbf{j}\} - (r_h L_1, r_h L_2, r_v L_3) + \mathbf{T} \tag{4}$$

where

$$\bar{\rho}_x(t) = -\bar{T}_x(t) + \bar{S}_x(t) \text{ and } \bar{\rho}_y(t) = -\bar{T}_y(t) + \bar{S}_y(t) \tag{5}$$

and g' is the reduced gravity $g\delta\rho/\rho_0$. Also, $\mathbf{i}$, $\mathbf{j}$ and $\mathbf{k}$ denote unit vectors in the x, y and z-directions. Friction at the bottom and at the side walls is parametrized as a Rayleigh damping, with the frictional coefficients $r_{h,v}$ and $\mathbf{T}$ is the boundary-averaged supplied torque, at the surface related to the torque of wind stress.

2.2 Evolution of density gradients

Equation (4) requires an expression for the buoyancy torque which, as Eq. (5) show, is determined by variations in the temperature field (as given in M94) and the salinity field. The equations for the temperature and salinity fields are equivalent, any dynamical difference between the two is introduced through a difference in their respective boundary conditions or in their diffusion coefficients. The equations for the salinity field can therefore be directly derived from M94's equations, and are given by

$$\frac{W^2}{12}\frac{d\bar{S}_x}{dt} + \frac{1}{2}L_3\bar{S}_y - \frac{1}{2}L_2\bar{S}_z = -K_h^S\bar{S}_x + F_{*S}^x \tag{6a}$$

$$\frac{W^2}{12}\frac{d\bar{S}_y}{dt} + \frac{1}{2}L_1\bar{S}_z - \frac{1}{2}L_3\bar{S}_x = -K_h^S\bar{S}_x + F_{*S}^y \tag{6b}$$

$$\frac{H^2}{12}\frac{d\bar{S}_z}{dt} + \frac{1}{2}L_2\bar{S}_x - \frac{1}{2}L_1\bar{S}_y = -K_v^S\bar{S}_x + F_{*S}^z \tag{6c}$$

where K_h^S and K_v^S are the horizontal and vertical turbulent diffusivities of salt. The forcing at the surface, $z = H/2$, is

$$\mathbf{F}_{*S} = (F_{*S}^x, F_{*S}^y, F_{*S}^z) = \frac{1}{V}\int\int\left(x, y, \frac{H}{2}\right)Q_{*S}dxdy, \tag{7}$$

where Q_{*S} is the (virtual) salt flux (per unit mass). Analogous expressions hold for the moments of the buoyancy flux due to temperature fluctuations.

These evolution equations require a description of the (virtual) salt flux $\mathbf{F}_{*S}$ and heat flux $\mathbf{F}_{*T}$. The common procedure is to simply prescribe the virtual salt flux and restore temperature to climatic fields (Bryan 1986; Marotzke et al. 1988; Weaver and Hughes 1992; Weaver et al. 1993). Here the boundary condition on temperature will be a prescribed (zero net) heat flux instead of a restoring law, while the salt flux is coupled to the sea surface temperature. It is the model's dynamics which generates climatic fields.

There are some shortcomings inherent to this formulation. The meridional extent on which this model remains valid is limited. The use of the f-plane approximation is one reason for it. Another reason is that the application of an accurate evaporation-precipitation distribution with its increased precipitation in the tropics and in polar areas is not within the scope of the present model formulation, especially not the intricate atmospheric dynamics responsible for the average precipitation patterns. We suggest therefore that a valid application of the model extends from subtropical to subpolar areas. Another limitation of the model is that boundary layers are assumed to be present, but the model is not capable of resolving them, their effects being only crudely represented in terms of Rayleigh damping and Newtonian cooling.

3 Boundary conditions

3.1 Heat and virtual salt flux

In the parametrization of the heat and (virtual) salt flux, presented here, a static atmosphere is assumed with no heat capacity and lacking the ability to contain water vapour. Although the strength and spatial structure of ocean-atmosphere fluxes is dependent on atmospheric dynamics, we aim at the simplest possible representation of the SST-evaporation feedback. As in numerous other studies on thermohaline ocean circulation, the atmosphere will be treated as a passive element. Therefore, we assume that water vapour spreads out evenly over the basin and precipitates instantaneously. The feedback between ocean dynamics and atmospheric transport is excluded as well as the effects evaporation has on the radiation budget due to formation of clouds.

The total heat flux at the Earth's surface is the sum of the longwave radiation, latent heat flux, sensible heat flux and absorption of solar radiation. On a global scale, the incoming (absorbed) solar radiation is balanced by an average outgoing longwave flux of the same amount. However, solar radiation falls mainly in low latitudes while longwave radiation is more uniformly distributed over the Earth (Charnock 1994). This results in heating of equatorial regions and cooling of polar areas. This meridionally varying net heatflux will be assumed to be linearly dependent on latitude in view of the lowest order moments approach, where the characteristic meridional difference in the net heatflux will be termed Q_{sun}.

The temperature dependence of the evaporation E is written in terms of a truncated Taylor series expanded about a reference temperature T_0 and can be found elsewhere (Haney 1971; Gill 1982). Here the result is given;

$$E(T; T_0) = a[e_s^0 + e_s^1(T_* - T_0)] \tag{8}$$

with

$$e_s^0 \equiv e_s(T_0) \text{ and } e_s^1 \equiv \frac{de_s(T)}{dT}\Big|_{T_0} = \frac{L_v e_s(T_0)}{R_v T_0^2}.$$

The function $e_s(T)$ is the saturated water vapour pressure and L_v and R_v are the latent heat of evaporation and the gas constant for dry air. The constant a is the product of the density of air at standard pressure and temperature, the Dalton number (Gill 1982), the windspeed (at anemometer level) and the ratio of molecular weights of water and dry air divided by the air pressure at the sea surface, all combined in one parameter for notational ease. It is desirable to have no net moisture flux. Precipitation P, a constant in time and space, is chosen such that

$$\int (E(T_*, T_0) - P)\,\mathrm{d}x\mathrm{d}y = 0 \tag{9}$$

(where integration extends over the entire basin surface). The temperature difference $T_* - T_0$ is written in a Taylor expansion, retaining only linear terms, which implies that evaporation, due only to the background state, is in balance with precipitation, $E(T_0; T_0) = P$: excess evaporation in some areas is balanced by decreased evaporation in other areas, parametrizing moisture transport through the atmosphere. Expressions for the dimensional heat and salt flux now read:

$$Q_{*T} = -\frac{y_*}{W} Q_{\mathrm{sun}} + L_v E(T_*, T_0) \tag{10a}$$

$$Q_{*S} = \frac{S_0}{\rho_0}(E(T_*, T_0) - P) \tag{10b}$$

with S_0 and ρ_0 respectively the ocean background salinity and density (constant in time and space). Note that the constant term in the Taylor expansion of the evaporation E in Eq. (10a) will only be relevant for the radiation balance of the background state.

The latent heat flux is much larger than the sensible heat flux (Charnock 1994) and the sensible heat flux will therefore be ignored in this study.

The simple relation (8) is derived under several simplifications. The validity of these assumptions can be established by comparing Eq (8) with measurements, keeping in mind the limited meridional extent to which this model can be applied. With Eq (8) and ocean-like parameters of Table 1, we find, with a meridional surface temperature contrast of $\simeq 20\,^{\circ}\mathrm{C}$, a meridional difference in evaporation minus precipitation $\Delta(E-P) \simeq 3.7\, my^{-1}$. Schmitt et al. (1989) gives realistic value for $\Delta(E-P) \simeq 1.25\, my^{-1}$. The characteristic value of evaporation-precipitation used in this model thus overestimates realistic values only by a factor of 3. A characteristic value for the buoyancy flux due to the solar heat flux and latent heat flux combined is $\simeq 17 \times 10^{-9}\, ms^{-1}$. A realistic value for just the thermal buoyancy flux is about $10\text{–}15 \times 10^{-9}\, ms^{-1}$ (Schmitt et al. 1989). A characteristic value for the model's haline buoyancy flux is $\simeq 3 \times 10^{-9}\, ms^{-1}$, which is about three times higher than measured values (Schmitt et al. 1989). This simple parametrization of SST-dependent evaporation therefore produces a thermal and haline buoyancy flux which is of the same order of magnitude as characteristic (present-day) values.

3.2 Scaling and presentation of the three-dimensional thermohaline ocean circulation model

The 'driving force' behind thermohaline ocean dynamics is the meridional variation in incoming solar radiation minus outgoing longwave radiation. This variation, which we termed Q_{sun}, is the most natural scale for scaling buoyancy input. The total buoyancy flux, regardless whether it is brought about by heat or salt fluxes, is scaled with

$$\frac{\alpha}{c_w \rho_0^2} Q_{sun} \tag{11}$$

where c_w is specific heat of sea water. The buoyancy flux due to respectively the heat and salt flux is:

$$\frac{\alpha}{c_w \rho_0^2}\left[\frac{-y_*}{W} Q_{sun} + L_v E(T; T_0)\right], \frac{\beta S_0}{\rho_0^2} E(T; T_0) \tag{12}$$

We employ the following scales: $(x, y, z, t) = (W, W, H, W^2/K_h^T)$, $(u, v, w) = (K_h^T/W, K_h^T/W, K_h^T/W^2)$ and $\delta\rho = (12\rho_0 K_h^T r_h/gH)$. The buoyancy flux due to the first moments of the heat and salt fluxes is, with Eqs. (10a, b) and Eqs. (1) and (2), applied to temperature T and, splitting off the dimensional factor $\alpha Q_{sun}/c_w\rho_0^2$,

$$Q_T = [-y + \xi(x\bar{T}_x + y\bar{T}_y)] \tag{13a}$$

and

$$Q_S = [\gamma(x\bar{T}_x + y\bar{T}_y)] \tag{13b}$$

respectively. Furthermore,

$$\xi = \frac{L_v a e_s^1}{Q_{sun}} \frac{\widehat{\delta\rho}}{\alpha} \text{ and } \frac{\gamma}{\xi} = \frac{c_w \beta S_0}{\alpha L_v},$$

where $\widehat{\delta\rho}$, introduced by scaling the surface temperature anomaly, is a characteristic density anomaly in the mixed layer. The scaling of the temperature anomaly introduced in Eq. (1) is only applicable to the interior of the ocean, and its numerical value is therefore very small (Table 1). A parametrization of processes like evaporation and precipitation must be scaled with scales appropriate for the ocean mixed layer, although the model does not explicitly contain mixed layer dynamics. Typical temperature anomalies in the ocean's mixed-layer are much larger than those in the ocean's interior; the use of the temperature anomaly scale valid in the interior of the ocean would result in a gross underestimation of the latent heat flux

Table 1 Characteristic values and units of dimensional quantities

Parameter	Meaning	Value	Unit
α	Thermal expansion coefficient	0.14	$kgm^{-3}K^{-1}$
β	Haline expansion coefficient	0.78	$kgm^{-3}psu^{-1}$
L_v	Latent heat of evaporation	2.5×10^6	Jkg^{-1}
ρ_*	Density of sea water	10^3	kgm^{-3}
c_w	Specific heat of sea water	4×10^3	$Jkg^{-1}K^{-1}$
R_v	Gas constant for dry air	287	$Jkg^{-1}K^{-1}$
$E(T;T_0)$	Evaporation rate	–	$kgm^{-2}s^{-1}$
$P(T_0)$	Precipitation rate	–	$kgm^{-2}s^{-1}$
$e_s(T)$	Saturated water vapour pressure	–	$mbar$
a	Constant relating evaporation to $e_s(T)$	4.67×10^{-6}	$kgm^{-2}s^{-1}mbar^{-1}$
T_0	Reference temperature	9	$^\circ C$
S_0	Reference salinity	35	psu
e_s^0	Saturated water vapour pressure at temperature T_0	11.47	$mbar$
e_s^1	Derivative of $e_s(T)$ with respect to T at temperature T_0	1.26	$mbar^\circ C^{-1}$
$\hat{u}$	Frictional (wind) velocity	10^{-2}	ms^{-1}
$K_h^{T,S}$	Horizontal eddy diffusion coefficient	10^2	m^2s^{-1}
$K_v^{T,S}$	Vertical eddy diffusion coefficient	10^{-4}	m^2s^{-1}
r_h, r_v	Horizontal and vertical frictional damping rates	10^{-6}	s^{-1}
Q_{sun}	Meridional difference in (net) solar radiation	200	Wm^{-2}
W	Horizontal basin size	5×10^6	m
H	Vertical basin size	5×10^3	m
h	Depth of the mixed layer	50	m
g	Gravitational acceleration	10	ms^{-2}
f	Coriolis parameter	10^{-4}	s^{-1}
$\delta\rho$	Density perturbation in the interior of the ocean	2.4×10^{-5}	kgm^{-3}
$\widehat{\delta\rho}$	Density perturbation in the mixed-layer of the ocean	0.7	kgm^{-3}

and the (virtual) salt flux. A proper time scale for the surface temperature anomaly is provided by the thermal wind balance and yields: fW^2/gh, with g the acceleration of gravity and h the depth of the mixed layer. A subsequent scale for the density anomaly itself in the mixed layer is given by an equilibrium between the rate of change of density and (thermal) bouyancy flux. This gives: $\widehat{\delta\rho} = \alpha Q_{sun} fW^2/\rho_0 g c_w h^2$. The parameters ξ and γ combine the (relative) effect of evaporation on the buoyancy, ξ is the effect of the latent heat flux on the buoyancy, γ is the effect of the (virtual) salt flux due to evaporation–precipitation on the buoyancy. The buoyancy flux for the lowest-order, basin-sized dynamics is the buoyancy flux into the mixed layer projected on the first density mode, as in Eq. (7).

Numerical factors are absorbed in Eqs (4) and (6) by rescaling time with a factor 1/12 and $\delta\rho$ and $\mathbf{u}$ with a factor 2.

Adopting the scales given (and by M94) gives the following simple model for the three dimensional thermohaline circulation:

$$Pr^{-1}\frac{d\mathbf{L}}{dt} + f'\mathbf{k}\times\mathbf{L} = -\bar{\rho}_y(t)\mathbf{i} + \bar{\rho}_x(t)\mathbf{j} - (L_1, L_2, rL_3) + \hat{T}\mathbf{T} \quad (14a)$$

$$\frac{d\nabla\bar{T}}{dt} + \nabla\bar{T}\times\mathbf{L} = -(\bar{T}_x, \bar{T}_y, \mu^T\bar{T}_z) + Ra\mathbf{F}_T \quad (14b)$$

$$\frac{d\nabla\bar{S}}{dt} + \nabla\bar{S}\times\mathbf{L} = -\lambda(\bar{S}_x, \bar{S}_y, \mu s\bar{S}_z) + Ra\mathbf{F}_S \quad (14c)$$

with $\bar{\rho} = -\bar{T} + \bar{S}$. Note that the salt flux vector $\mathbf{F}_S$, and its thermal analogue $\mathbf{F}_T$ are defined in Eq. (7) with $Q_{T,S}$ as in Eq. (13).

Here $Pr = r_h W^2/12K_h^T$ denotes the Prandtl number, $f' = f/2r_h$ the scaled Coriolis parameter, $r = r_v/r_h$, the ratio of the frictional time scales of horizontal and vertical angular momentum, and $\hat{T} = \hat{u}^2 W/2r_h K_h^T H$ the dimensionless magnitude of the torque exerted by the windstress. The Lewis number $\lambda = K_h^S/K_h^T$ is the ratio of horizontal turbulent diffusivities of salt and heat. The ratio of the vertical and horizontal diffusion time scales for heat and salt are denoted by $\mu^T = K_v^T W^2/K_h^T H^2$ and $\mu^S = K_v^S W^2/K_h^S H^2$. It is physically reasonable that the ratio of vertical to horizontal turbulent diffusion of heat equals that of salt, $\mu^T = \mu^S$. The flux-Rayleigh number Ra, a ratio of the driving buoyancy force and the diffusive process that tends to decrease the density gradients, is given by $Ra = \alpha Q_{sun} W^2/K_h^T c_w \rho_0^2 H$.

Taking the ocean-like parameter values of Table 1, we find that typical magnitudes of the non-dimensional numbers are: $Pr = 2\times10^4$, $f' = 50$, $r = 1$, $\mu^T = \mu^S \equiv \mu = 1$, $\hat{T} = 500$ and $Ra = 0.35$, while the dimensional time scale $W^2/12K_h^T$ is of $O(500)$ years. The relative strength of the latent heat flux on buoyancy, captured in the parameter ξ, is 0.37, while γ/ξ is 1/4 for typical surface values (Gill 1982). The dimensionless parameters and the model variables are recapitulated in Tables 2 and 3.

One of the drawbacks of simple models is that they parametrize several processes which are relevant for ocean dynamics. These

Table 2 Characteristic values of dimensionless quantities

Parameter	Meaning	Value
ξ	Relative strength of buoyancy flux due to latent heat	0.37
γ	Relative strength of buoyancy flux due to evaporation	0.093
Pr	Prandtl number	2×10^4
f'	Scaled Coriolis parameter	50
r	Ratio of horizontal and vertical frictional damping rates	1
$\hat{T}$	Magnitude of the windstress torque	500
λ	Lewis number	1
$\mu^{T,S} = \mu$	Vertical and horizontal diffusion time scales	1
Ra	Rayleigh number	0.35

Table 3 Model variables

Parameter	Meaning
$\mathbf{x} = (x, y, z)$	Position vector
$\mathbf{u} = (u, v, w)$	Velocity vector
$\mathbf{L} = (L_1, L_2, L_3)$	Basin-averaged angular momentum vector
$\mathbf{T}$	Boundary-averaged supplied wind torque
$\mathbf{F}_S$	Moments of the buoyancy flux due to salt variations
$\mathbf{F}_T$	Moments of the buoyancy flux due to heat variations
∇T	Temperature perturbation gradients
∇S	Salinity perturbation gradients
$\nabla\rho = \nabla S - \nabla T$	Density perturbation gradients

parametrizations produce consequently parameters whose precise numerical value can be subject to discussion, as the nature of the parametrizations themselves can be. Using parametrizations, it is not exactly known where in parameterspace the projection of 'reality' resides. Furthermore, modelling ocean dynamics under climatic circumstances other than the present one, implies a different choice of parameter setting. Therefore we propose to regard the characteristic numerical values of the parameters merely as a guideline: they can be subject to significant alteration without leaving the bounds of a realistic setting.

4 Model results

4.1 Circulation in the meridional plane: $f' = 0$

The study will be confined to the situation where the heat flux only consists of incoming solar radiation minus outgoing longwave radiation. The contribution of the latent heat flux to the total surface heat flux is, for the sake of simplicity, left out. With $f' = 0$ in Eq. (14) the circulations in the zonal and meridional planes decouple and the latter is described by

$$\bar{\rho}_y = -\bar{T}_y + \bar{S}_y;\ \bar{\rho}_z = -\bar{T}_z + \bar{S}_z \tag{15a}$$

$$Pr^{-1}\frac{dL_1}{dt} + \bar{\rho}_y = -L_1 \tag{15b}$$

$$\frac{d\bar{T}_y}{dt} + \bar{T}_z L_1 = -\bar{T}_y - Ra \tag{15c}$$

$$\frac{d\bar{T}_z}{dt} - \bar{T}_y L_1 = -\mu^T \bar{T}_z + Ra F_T^z \tag{15d}$$

$$\frac{d\bar{S}_y}{dt} + \bar{S}_z L_1 = -\lambda\bar{S}_y + \gamma Ra\bar{T}_y \tag{15e}$$

$$\frac{d\bar{S}_z}{dt} + \bar{S}_y L_1 = -\mu^S\lambda\bar{S}_z + Ra F_S^z \tag{15f}$$

Neglecting salinity, in Eq. (15 b–d) we recognize the Howard-Malkus loop (Malkus 1972; Welander 1986), if the lateral forcing terms are allowed to vanish. This loop is a thermal oscillator in which fluid in a ring, placed in the vertical, is differentially heated vertically. The buoyancy torque creates angular momentum, which advects the density field. On the other hand neglecting temperature, Eq. (15b, e–f) describe the same oscillator but with a haline character. The system (15) with no lateral forcing is therefore a loop oscillator with buoyancy generated by both thermal and haline forcing purely in the vertical. Malkus (1972) remarks on the equivalence of his equations to those of Lorenz (1963). Winton and Sarachik (1993) refer to a loop model for the description of a mechanism which leads to periodic behaviour. The loop model driven by both heat and freshwater fluxes has been discussed by Dewar and Huang (1995) as to the sensitivity to the boundary condition on salinity.

The external forcing in Eq. (15c) of the temperature field has been reduced to a constant term, producing a balance between (net) incoming/outgoing solar radiation, inertia, advection and Newtonian cooling. The effect of evaporation on the salinity has been included at a very elementary level, expressing the (virtual) salt flux in terms of the meridional temperature gradient. If it is assumed that there is no inertia in the angular momentum equation ($Pr \to \infty$) Stommel's (1961) dynamics is retrieved in which the buoyancy torque balances the frictional torque:

$$\bar{\rho}_y = -L_1$$

Equation (15) carries information about the vertical salinity and heat structure, unlike Stommel's. When (see M94) it is assumed that changes in the vertical density gradient occur instantaneously and the net heat and salt fluxes F_T^z and F_S^z vanish, as seems likely in a large-scale basin (M94), Eq. (15) can be reduced to

$$\dot{\bar{T}}_y = -\bar{T}_y - \frac{L_1^2\bar{T}_y}{\mu^T} - Ra \tag{16a}$$

$$\dot{\bar{S}}_y = -\lambda\bar{S}_y - \frac{L_1^2\bar{S}_y}{\mu^S\lambda} + \gamma Ra\bar{T}_y \tag{16b}$$

where the dot is an abbreviated notation for the time derivative. It is assumed that the Lewis number is $\lambda \simeq 1$ (Källén and Huang 1987; Thual and McWilliams 1992). This, along with the other assumptions, removes the possibility of periodic motion in this 2-D limit, as can be shown with Bendixson's criterion (Guckenheimer and Holmes 1983). The absence of periodic motion in this limit has recently also been remarked by Ruddick and Zhang (1996).

In accordance with Stommel's model, multiple equilibria are found due to the different boundary conditions employed for temperature and salinity. Equation (16) with $\lambda = 1$ and $\gamma = 0.1$, produces a state with a branch of stable stationary solutions in the Ra-parameter (sub) space with a positive meridional density gradient, corresponding to a thermal flow regime, and a branch of stable stationary solutions with negative meridional gradients. The latter branch corresponds to a haline flow regime. These two branches of solutions

are joined by a branch of unstable solutions. Both flow regimes can coexist, similar to the results Stommel (1961) found, for a limited range of the parameter *Ra*.

If in Eq. (16) the virtual salt flux is prescribed instead of being coupled to the temperature gradient $\bar{T}_y$, the mathematical structure of Stommel's (1961) 2-box model is retrieved, with this difference that the strength of the circulation appears as a squared term instead of the absolute values used by Stommel (see M94).

4.2 Circulation in the 3-D basin, $f' \neq 0$

Including rotation in the limit $Pr \to \infty$ (Weaver and Sarachik 1991; Wright and Stocker 1991; Thual and McWilliams 1992) and with no direct wind forcing, the following equations are found

$$L_1 = f' \bar{\rho}_x - \bar{\rho}_y \tag{17a}$$

$$L_2 = f' \bar{\rho}_y + \bar{\rho}_x \tag{17b}$$

$$\dot{\bar{S}}_x = \bar{S}_z L_2 - \lambda \bar{S}_x \tag{17c}$$

$$\dot{\bar{S}}_y = \bar{S}_z L_1 - \lambda \bar{S}_y + \gamma Ra \bar{T}_y \tag{17d}$$

$$\dot{\bar{S}}_z = \bar{S}_y L_1 - \bar{S}_x L_2 - \lambda \mu \bar{S}_z \tag{17e}$$

$$\dot{\bar{T}}_x = \bar{T}_z L_2 - \bar{T}_x \tag{17f}$$

$$\dot{\bar{T}}_y = -\bar{T}_z L_1 - \bar{T}_y - \frac{Ra}{(1+f'^2)} \tag{17g}$$

$$\dot{\bar{T}}_z = \bar{T}_y L_1 - \bar{T}_x L_2 - \mu \bar{T}_z \tag{17h}$$

where no wind-stress torque and differential heating and saltening/freshening in the east-west direction ($F_T^x = F_S^x = 0$) is assumed. Differential heat and salt fluxes in the vertical are neglected, in order to conserve heat and salt ($F_T^z, F_S^z = 0$). Inclusion of these fluxes would result in uniform, basinwide surface cooling/warming and precipitation/evaporation respectively (see M94). Furthermore, $\bar{S}$ and $\bar{T}$ were redefined by multiplying them with $1/(1+f'^2)$.

Although the existence of multiple equilibria is one of the features of thermohaline circulation in double hemispheric 2-D and 3-D models (Bryan 1986; Cessi and Young 1992; Thual and McWilliams 1992; Quon and Ghil 1992, 1995), multiple steady states appear to be absent in our single-hemisphere 3-D model for present-day values of the parameters. Unlike the non-rotating 2-D case presented above, the transition between the thermal regime and the haline regime in the rotating case is gradual and smooth without hysteresis. The hysteresis gradually diminishes and eventually disappears when increasing f'. Hysteresis is no longer present for $f' = 2.05$, under the parameter setting: $\mu = 3$, $\gamma = 0.1$ and $\lambda = 1$. The stable equilibria of the thermohaline circulation which coexist for the same forcing in a double hemispherical setting are the one-cell pole-to-pole solutions which originate from symmetrical two-cell solutions through a symmetry breaking bifurcation (e.g. Dijkstra and Molemaker 1997). It is clear that the present single-hemispheric model cannot produce the pole-to-pole solution being limited to a single hemisphere, but is only capable of producing (one half) of the symmetrical two-cell solutions. However, Weaver et al. (1993) found multiple equilibria, all of thermal nature, even in their single hemispherical GCM runs. We expect this to be due to wind. M94 showed that in a thermally-driven single-hemisphere ocean, multiple equilibria are produced by constant windforcing. The precise effects of windforcing on the bifurcation structure are not addressed here.

4.2.1 Parameter setting

Choosing $\mu = 3$, $f' = 10$, $\gamma = 20$ and $\lambda = 1$ places the equilibria of the system firmly in the haline regime. This particular parameter setting, that will be motivated later, is used throughout the remainder of this study. The parameter setting with $\gamma = 20$ is far removed from a parameter choice based on the present-day situation in the Atlantic and it can probably not be identified with past climates either. Since the parametrization of the salt flux boundary condition is quite different from the heat flux boundary condition, it seems reasonable to study the model in the salt dominated limit in complement to the thermal limit, sketched in M94. Future studies must determine which aspects of the behaviour in these extreme limits are robust enough to survive into a more realistic parameter regime. We do feel, however, that parameter values in the model should be varied in order for the model to be applicable to circumstances different from those in present-day climatic regimes. It is not possible to include the entire spectrum of climate variability within a simple model of the thermohaline ocean circulation and a parametrized atmospheric response to ocean dynamics with one single parameter setting. This is obvious for changes in the orbital parameters of the Earth which directly affect the net amount and the distribution of incoming solar radiation. Moreover, it is argued (Pestiaux et al. 1987) that the precessional contribution to the forcing interacts strongly with the SST-precipitation feedback. This interaction is beyond the reach of the SST-evaporation feedback parametrization used here. In addition, the latter parametrization condenses several physical processes, and in the resulting parameter, γ, values for e.g. windspeed at anemometer level (Haney 1971; Gill 1982) and the depth of the mixed-layer are absorbed. Evidence suggests, however, that mixed-layer depth in the equatorial Atlantic is controlled by variations in the tropical easterlies, forced by the precessional component of orbital insolation (McIntyre et al. 1989; Molfino and McIntyre 1990), causing a variation in the numerical value of this parameter.

An example of an entirely different climate, and therefore a candidate for an extreme parameter setting, not necessarily the current choice, is the Cretaceous. In

the early Cretaceous, land masses or very shallow seas still separated the Atlantic and the Tethys from the polar seas, prohibiting the formation and southward flow of cold and oxygenated deep water, resulting in a sluggish circulation (Baudin and Herbin 1995). Anoxic depositions may have been further supported by the generation of oxygen-deficient, saline bottom water in strongly evaporetic low latitudes (Brass et al. 1982; Sinninghe Damsté and Köster 1998). Furthermore, paleontological and sedimentological data suggest that climates in high latitudes during the mid-Cretaceous were generally warmer than at present (Crowley and North 1991). Oxygen isotope records indicate that the Cretaceous intermediate - deep waters were about 15 °C warmer than at present (Douglas and Woodruff 1981), also SST-values in mid and high latitudes differed by as much as 10–15 °C (Barron 1983; Barron and Washington 1985). An increased SST has a profound effect on the saturated water vapour pressure $e_s(T)$, since warm air can contain much more water (Brutsaert 1982), increasing the cloudiness. It is likely, therefore, that in the Cretaceous the relative importance of the evaporation - precipitation balance was more significant.

4.2.2 Steady states

The bifurcation structure of the model is determined with AUTO (Doedel 1981), a software package which computes branches of stable and unstable equilibria and locates and classifies bifurcations. For $Ra < 2.87$ there is a steady state solution. For small values of Ra we find a thermally driven circulation. For slightly higher values of Ra, this turns into a haline circulation with $\bar{\rho}_x > 0$ and $\bar{\rho}_y < 0$, corresponding to surface flow directed to the south-west. At $Ra \simeq 2.87$ a Hopf-bifurcation occurs and a stable periodic solution emerges. This oscillation corresponds to a salinity anomaly which is advected with the overturning circulation. If the forcing is strong enough, the balance between dissipation and forcing prevents the salt anomaly from vanishing. The anomaly affects the density gradients and it influences the strength and direction of the overturning circulation depending on its position, although the surface flow remains directed roughly towards the south-west. It can be followed through the basin by analyzing the time dependence of the salinity gradients and reconstructing its path (Fig. 1).

4.2.3 Periodic solutions

The oscillatory cycle can be described starting from the moment that the total overturning is for instance at a minimum. The prescribed heat flux in combination with a weak circulation will decrease the negative meridional temperature gradient $\bar{T}_y$, increasing the temperature contrast between southern and northern regions. This results, due to the coupling of the virtual salt flux with $\bar{T}_y$, in an increasing salinity at the southern edge of the basin and a decreasing salinity at the northern edge, which, by geostrophy, results in its turn, in an increase of zonal overturning strength (density is dominated by salinity). Because of this strong negative overturning in the zonal plane, the zonal density gradient will increase, directly followed by an increase in meridional overturning L_1. The total overturning has just passed a maximimum by now, decreasing the meridional temperature contrast.

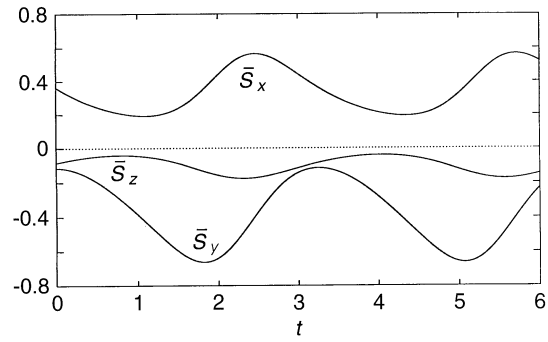

Fig. 1 The periodic time dependence of the three salinity derivatives for $Ra = 3.08$. Periodic motion for this Ra-number corresponds with advection of anomalously saline water through the basin. Parameters are: $\mu = 3, f' = 10, \gamma = 20$ and $\lambda = 1$

A key element in the occurrence of these cycles is inertia, and a time lag between meridional overturning and a meridional density gradient is caused by the geostrophic coupling. An increase in meridional density gradient induces, with no time lag, a zonal overturning. Consequently, a zonal density gradient is established which provides, in its turn, a meridional circulation.

Probably due to the haline character of the flow we find that the overturning is rather sluggish. In the meridional plane it varies for $Ra = 3.08$ between 2.2 and 6.0 Sv ($1\ Sv = 10^6\ m^3\ s^{-1}$) and in the zonal plane between -0.8 and $-6.0\ Sv$. The salinity gradients vary between -1.0×10^{-7} and $-1.9 \times 10^{-8}\ psu\, m^{-1}$, corresponding to a meridional contrast over the basin length ($5 \times 10^6\ m$) of -0.5 to $-0.1\ psu$. The temperature gradients vary between to -1.7×10^{-8} to $-0.6 \times 10^{-8}\ ^\circ C m^{-1}$, corresponding to a meridional contrast over the basin length of -0.09 to -0.03 °C. These values are salinity and temperature differences in the *interior* of the basin. Considering the slow circulation and the modest salinity and temperature gradients, the period of the motion is consequently very long. For $Ra = 3.08$ it is approximately three non-dimensional time units, corresponding to about 1500 y.

This mechanism behind oscillatory equilibria, advection of a blob of anomalously saline water, has been encountered in several studies (Mikolajewicz and Maier-Reimer 1990; Mysak et al. 1993; Winton and

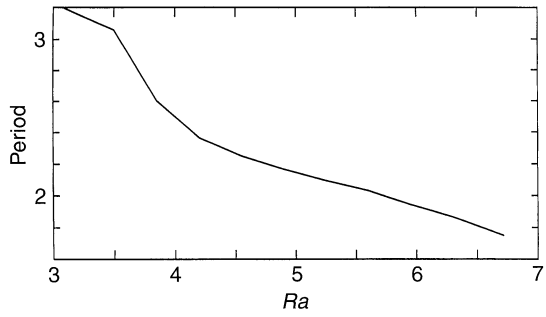

Fig. 2 Dependence of the period of the oscillatory motion on the forcing parameter *Ra*. Parameters are: $\mu = 3$, $f' = 10$, $\gamma = 20$ and $\lambda = 1$. For $Ra = 4.2$ and onwards, the period is nearly linearly dependent on *Ra*. The period of the motion is given in non-dimensional time units

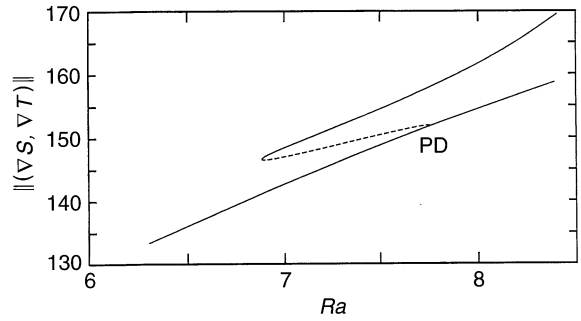

Fig. 3 Bifurcation diagram giving the norm of periodic solutions $\|(\nabla S, \nabla T)\|$ as a function of the forcing parameter *Ra*. The norm $\|(\nabla S, \nabla T)\|$ is defined as the square root of the sum of all squared components of $(\nabla S, \nabla T)$ averaged over one period ρ: $\|(\nabla S, \nabla T)\|^2 = \frac{1}{\rho} \int_0^\rho (\nabla S \cdot \nabla S + \nabla T \cdot \nabla T) dt$. Solid lines indicate branches of stable periodic equilibria, the dashed line indicates unstable periodic equilibria. Parameters are: $\mu = 3$, $f' = 10$, $\gamma = 20$ and $\lambda = 1$. At the period-doubling bifurcation (marked PD) a stable branch appears. This branch turns unstable at a limit point, where the distance in parameterspace between the period-doubling bifurcation and the limit point is very small

Sarachik 1993; Huang and Chou 1994) both in 2-D and 3-D models.

For values of *Ra* smaller than the one at which the Hopf bifurcation occurs, this oscillation is preshadowed by the nature of the static equilibrium, a *spiral* sink. A disturbance from this equilibrium (a salt anomaly) is advected with the overturning circulation, affecting the circulation itself in strength and direction until diffusion has annihilated the anomaly and the motion is stationary again.

The direction of the motion changes gradually with increasing *Ra*. Due to inertia of the system it overshoots for larger values of *Ra*, which results in sign changes of meridional and zonal density gradients. The circulation becomes more vigorous, increasing its overturning rate and decreasing the motion's period. An interesting aspect of this oscillatory motion is that the period of the motion decreases almost linearly with the forcing strength *Ra*, from $Ra = 4.2$ onwards (Fig. 2), agreeing with other studies (Huang and Chou 1994; Dewar and Huang 1995).

At $Ra \simeq 7.77$ a period-doubling (subharmonic bifurcation) occurs (Fig. 3). The bifurcated branch proceeds in decreasing *Ra* direction after it encountered a limit point. The bifurcated branch turns unstable after this limit point, to encounter a second limit point at $Ra \simeq 6.86$, where the periodic solution turns stable again and the branch of solutions proceeds in increasing *Ra* direction. This feature results in a situation where for a range of *Ra*-values two stable periodic orbits exist, one with a period of say τ and with a relatively low maximum overturning, and another with a period of about 2τ and with a relatively high maximum overturning.

We now discuss the different phases of the 2τ cycle. The density difference between bottom and surface gradually decreases until the basin has a near uniform vertical density field (Fig. 4a). The strength of the

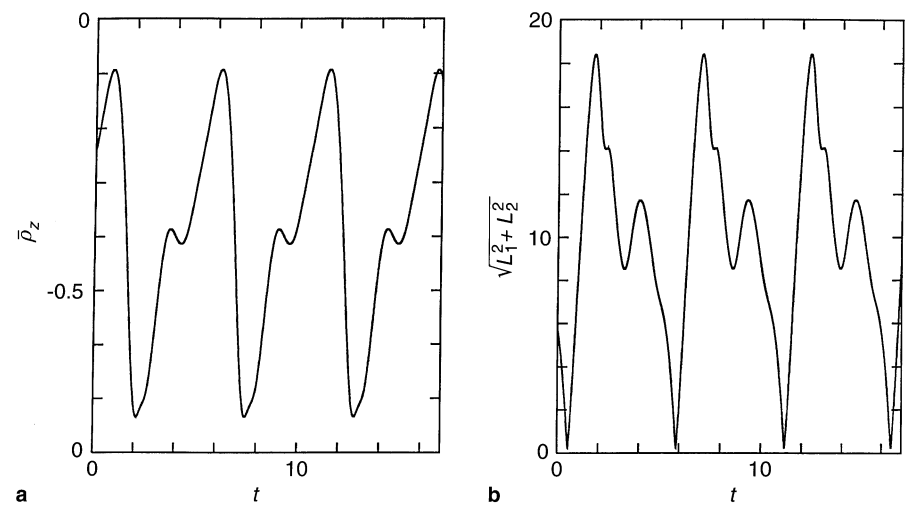

Fig. 4 Time evolution of the vertical density gradient **a** and of $\sqrt{L_1^2 + L_2^2}$ **b** denoting a measure for the strength of the circulation for $Ra = 7.7$. A period of gradual relaxation of the vertical density contrast along with a diminishing circulation strength is followed by short intervals during which the vertical density contrast and the strength of the circulation increases dramatically. Parameters are: $\mu = 3$, $f' = 10$, $\gamma = 20$ and $\lambda = 1$

circulation decreases reaching this state and diffusion slowly relaxes the salinity gradients in zonal and meridional direction. Diffusion is the dominant proces in this part of the cycle, in analogy with Wright and Stocker (1991). In this phase the basin-averaged vertical stratification diminishes. The slow circulation allows an increasing temperature gradient between the northern and southern edges of the basin to be build up, because of the ever-present heat flux. The forcing on the meridional salinity gradient $\bar{S}_y$ therefore increases and consequently $\bar{S}_y$ and the zonal overturning L_2 will rapidly become more negative. The strong zonal overturning precedes in its turn an increasing zonal salinity gradient $\bar{S}_x$ and a consequently increasing meridional overturning L_1. This phase in the cycle corresponds to a massive increase in total overturning circulation (Fig. 4b). The motion accelerates, the vertical density contrast is increased and the haline character of the dynamics starts to dominate the evolution of the system. Due to inertia of the temperature and salinity fields, the system overshoots while adjusting itself to this increase in circulation strength, and a gradual relaxing of the three density gradients follows, eventually closing the cycle.

This oscillatory motion distinguishes itself from salt anomaly advection in this model by the short phase with huge overturning and accompanying rapid restratification and the long phase where thermal and haline inertia and diffusion seem to be the dominant processes, leading to slowly diminishing transport rates and weakening stratification. Oscillatory motion which can be identified with the advection of a salt anomaly on the other hand gives a much more regular and smooth behaviour. The first period-doubling bifurcation marks the transition between both regimes.

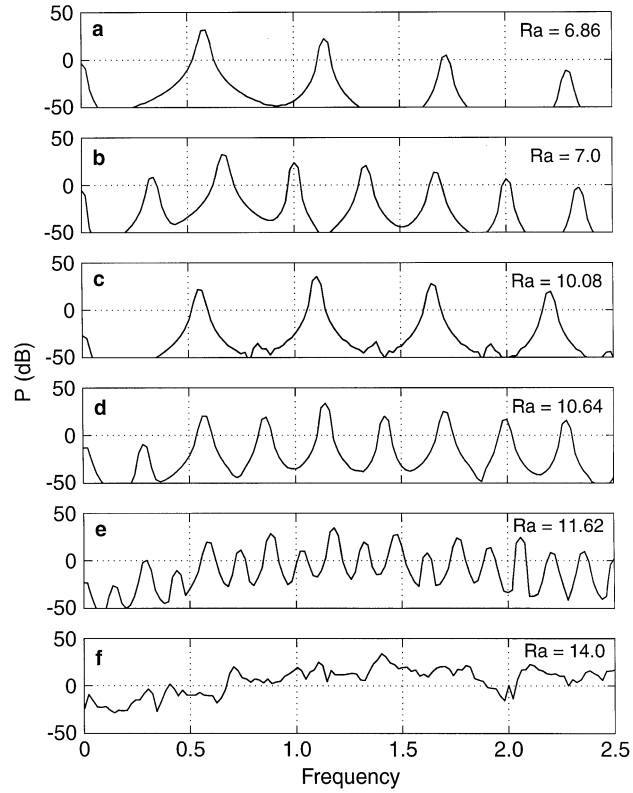

Fig. 5a–f Power spectral density P of the meridional density gradient which demonstrates the period-doubling cascade. At $Ra = 6.86$ **a** one frequency with its superharmonics is observed and for $Ra = 7.0$ **b** the first subharmonic has occurred. Notice that the fundamental frequency ($\simeq 0.58$) has shifted a bit to the right which is caused by the fact that the periodic solutions for $Ra = 6.86$ and $Ra = 7.0$ are not directly linked in parameter space: the frequency of the motion is not constant over the branch which unites these two equilibria. In Fig. **c–e** one observes the appearance of new subharmonics for increasing Ra. The other parameters are held constant at: $\mu = 3, f' = 10, \gamma = 20$ and $\lambda = 1$

4.2.4 *Chaotic motion*

For still larger values of Ra a cascade of period-doubling bifurcations occurs, which results in the appearance of chaotic motion (Fig. 5). For $Ra = 6.86$ one fundamental frequency is observed together with its superharmonics while for $Ra = 7.0$ the first subharmonic bifurcation has occurred. The frequency of the periodic solution has shifted to a slightly larger value. This is caused by the fact that the periodic solutions for $Ra = 6.86$ and $Ra = 7.0$ are not directly linked in parameter space. Increasing Ra clearly shows the appearance of more subharmonics, until in the chaotic regime ($Ra = 14.0$) energy ceases to be concentrated at distinct frequencies. The occurrence of chaos in the present model is also demonstrated in Fig. 6, where the largest non-zero Lyapunov exponent is plotted against Ra. A positive Lyapunov exponent indicates chaotic motion (Guckenheimer and Holmes 1983). The computation of the Lyapunov exponents is performed with

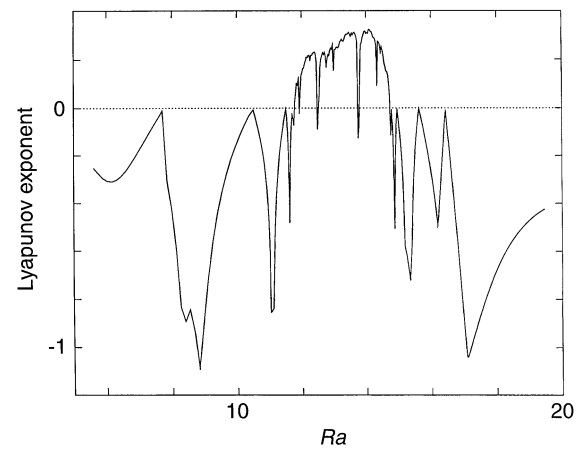

Fig. 6 Diagram of the largest non-zero Lyapunov exponent as a function of the forcing parameter Ra. A negative Lyapunov exponent indicates periodic motion whereas chaotic motion is characterized by a positive Lyapunov exponent. Values of Ra for which the Lyapunov exponent is zero indicate the appearance of a bifurcation. Chaotic motion occurs for a limited range of Ra and within this chaotic band we find islands with periodic motion. The other parameters are fixed at: $\mu = 3, f' = 10, \gamma = 20$ and $\lambda = 1$

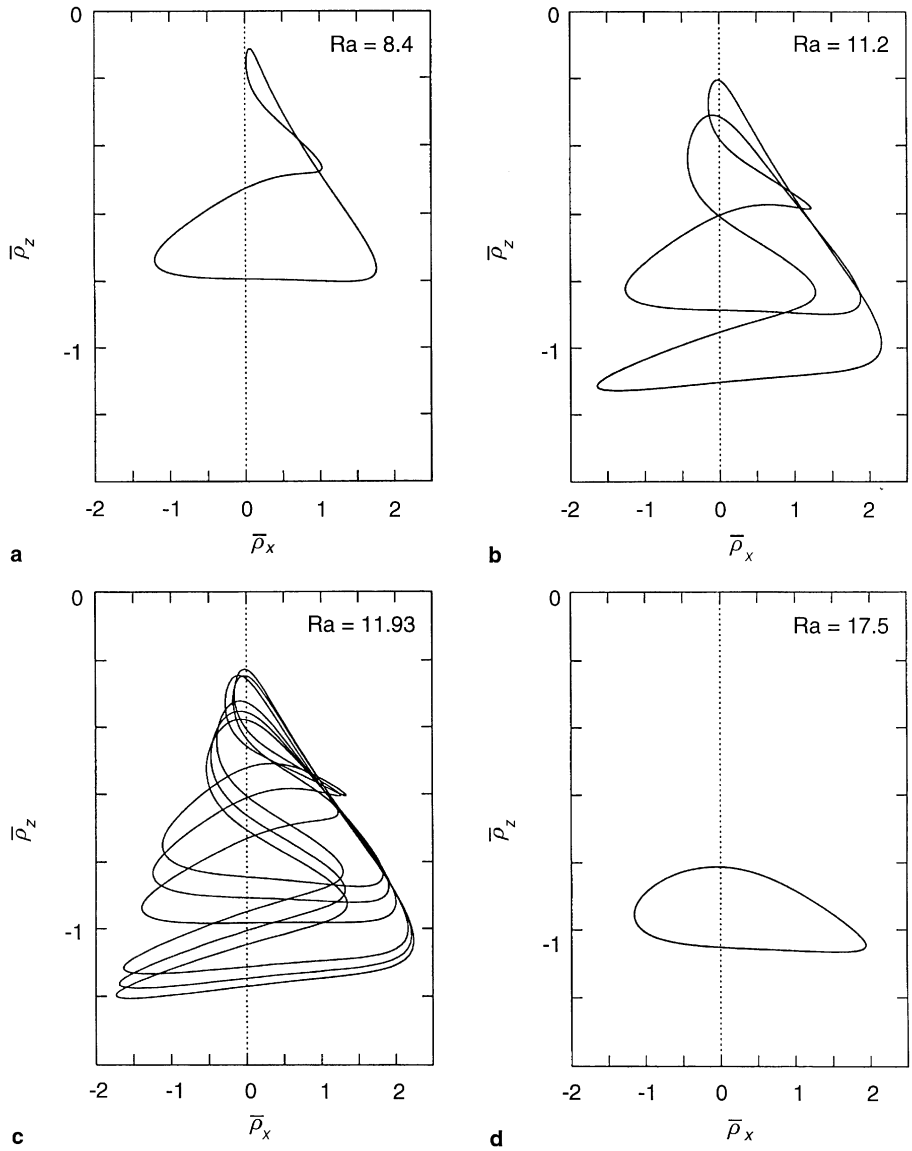

Fig. 7a–d The trajectories of the motion for resp. **a** $Ra = 8.4$, **b** $Ra = 11.2$ (corresponding to periodicity after the 1^{st} and 2^{nd} period-doubling bifurcations), **c** $Ra = 11.93$ (corresponding to the period-3 solution) and **d** $Ra = 17.5$ (corresponding to periodic motion in a regime with no chaotic motion but at higher values of the forcing parameter). The other parameters are fixed at: $\mu = 3, f' = 10, \gamma = 20$ and $\lambda = 1$

the code provided by Wolf et al. (1985). Chaos occurs in this model for a limited range of the forcing parameter Ra, and in the chaotic regime, periodic windows are found. In Fig. 7a–d trajectories are plotted for values of Ra at which respectively one ($Ra = 8.4$) or two ($Ra = 11.2$) subharmonic bifurcations have occurred. Also the trajectory of the period-3 solution ($Ra = 11.93$) and a trajectory of periodic motion which apparently occurs after a cascade of period-halvings ($Ra = 17.5$) is given. In Fig. 8a the intersection points of a trajectory in the chaotic regime ($Ra = 14.0$) with the plane $\bar{\rho}_x = 0$ is plotted (as a Poincaré plot). Part of a trajectory in the chaotic regime ($Ra = 14.0$) is plotted in Fig. 8b.

Notice that for all trajectories, the basin-averaged vertical density gradient remains statically stable. Statically stable states are also found in the chaotic regime, in contrast to the occurrence of chaos in purely convective models like the Lorenz (1963) model.

Chaotic motion has been encountered in several numerical studies on the thermohaline circulation (Weaver et al. 1993; Huang and Chou 1994). The occurrence of steady states, periodic motion and chaotic motion while retaining statically stable states in a very simplified model is a novel feature. Although these model results resemble those found by Huang and Chou (1994) in their single hemispherical, salt-only model, the only mechanism for periodic motion identified in their model is advection of anomalously saline water, in contrast to the present study. Although Huang and Chou also found a transition from periodic motion to chaotic motion and back while increasing their freshwater flux, a clear picture of their route to chaos has not been reported.

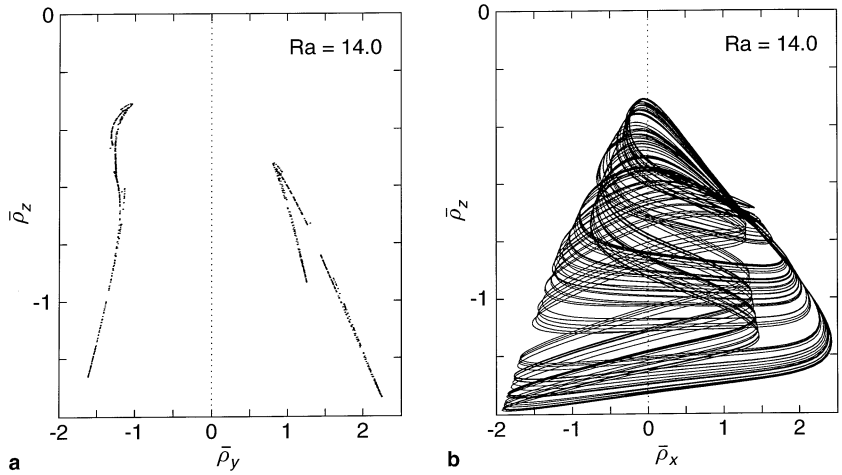

Fig. 8 **a** Intersection points of a trajectory in the chaotic regime ($Ra = 14.0$) with the plane $\bar{\rho}_x = 0$, a Poincaré plot, and **b** part of this trajectory. Other parameters are fixed at: $\mu = 3$, $f' = 10$, $\gamma = 20$ and $\lambda = 1$

5 Conclusion and discussion

In this study, we have presented a model for the thermohaline circulation, describing the evolution of the lowest moments of the momentum field and the heat and salinity fields in a rectangular f-plane ocean. As a low order projection of the Navier-Stokes equations, it combines the clarity of box models with essentials as rotation and wind-forcing, not covered in box models. This is where the strength of the model is found. Parameter space can be easily and accurately explored with this model, distinguishing qualitatively different circulation regimes of the thermohaline circulation.

As a consequence of the strongly parametrized way in which e.g. atmospheric processes or the dynamics of the mixed-layer are captured, the parameters in the model are not tightly fixed quantities. Modelling of different climates, unlike our present one, corresponds to choosing a different set of parameters.

We examined the sensitivity of this model in the salt-dominated limit to the strength of the thermal forcing. The model is subject to a thermal flux and a (virtual) salt flux, the latter coupled to the temperature of the basin through a simple parametrization of evaporation.

In the model's 2-D limit it is related to Stommel's (1961) box model. In this limit, a region in parameterspace is present in which multiple equilibria occur. The effect of increasing rotation is that the coexistence of a thermal and a haline solution gradually disappears. The transition between a thermal and a haline equilibrium with rotational coupling in this single hemispherical model, becomes gradual and smooth, without hysteresis.

The rotating salt-dominated 3-D circulation features a steady behaviour which can lead to selfsustained oscillations for higher values of the forcing strength. Periodic motion is due to advection of a salt anomaly increasing or decreasing the strength of the overturning circulation and varying its direction, depending on the position of the anomaly in the basin. For increased values of Ra, the motion becomes wilder and at $Ra \simeq 7.77$ a subharmonic bifurcation occurs. It is argued that this bifurcation marks the transition between two regimes of periodic motion. A regime where advection of a salt anomaly causes periodic motion is followed by a regime where the dynamics is sequentially driven by diffusion and inertia, leading to a relaxation of all density derivatives and a decreasing overturning, followed by a massive increase in overturning and adjustment processes. During this process, the basin-averaged vertical density structure remains statically stable. Model ocean dynamics may undergo a cascade of period-doubling bifurcations, resulting in a chaotic state, where the basin-averaged vertical density stratification remains nevertheless statically stable. Within the chaotic regime, islands of periodic motion exist. Chaos does not extend beyond a certain value of the control parameter Ra and this band of chaotic motion is followed by simple periodic motion.

This bifurcation study shows that the inclusion of rotational effects, even in this simple single hemispherical model, can lead to different dynamics compared to the rotationless 2-D results. The coexistence of a thermal and a haline equilibrium gradually disappears while increasing rotation, giving a smooth transition between both equilibria. Furthermore, it is argued that periodic motion, absent in our 2-D limit, results from two different mechanisms, and can lead to chaotic motion. In all states encountered in this model, (stable stationary, stable periodic and chaotic) the basin-averaged vertical density structure remained statically stable, for the discussed parameter setting. The results of this study indicate that low-order 2-D thermohaline circulation models, lacking the inertia associated with the rotational coupling of the zonal and meridional planes, might exclude some of the dynamical features of a rotating ocean.

Finally, the strong points of simple low-order models for thermohaline ocean circulation, conceptual clarity and easily interpretable results, combined with the inclusion of rotational effects, produce a model which recovers aspects of more advanced models. This paves the way for an analysis of thermohaline circulation, with a low-order model, in other relevant or more complex settings.

Acknowledgements Part of the computations were performed on the CRAY C-90 at the Academic Computer Centre (SARA), Amsterdam, the Netherlands, and sponsored by the National Computing Facilities Foundation (NCF) within project SC-212. We thank Dr H.A. Dijkstra (IMAU, Utrecht) for providing computing resources, and W. Weijer (IMAU, Utrecht) for discussions. We thank two (anonymous) referees for their constructive criticism. The investigations were supported by the Netherlands Geosciences Foundation (GOA) with financial aid from the Netherlands Organization for Scientific Research (NWO). This is contribution #3086 from the Netherlands Institute for Sea Research.

References

Baudin F, Herbin J-P (1995) Paleoenvironments and organic-rich facies deposition in the Tethys realm. In: Nairn AEM, Ricou L-E, Vrielynck B, Dercourt J (eds) The ocean basins and margins, vol 8: the Tethys ocean. Plenum Press, New York, pp 319–340

Barron EJ (1983) A warm, equable Cretaceous: the nature of the problem. Earth Sci Rev 19 : 305–338

Barron EJ, Washington WM (1985) Warm Cretaceous climates: high CO_2 as a plausible mechanism. In: Sundquist ET, Broecker WS (eds) The carbon cycle and atmospheric CO_2: natural variations Archean to present. Am Geophys Union, Washington D.C., pp 546–553

Brass GW, Southam JR, Peterson WH (1982) Warm saline bottom water in the ancient ocean. Nature 296 : 620–623

Broecker WS, Peteet DM, Rind D (1985) Does the ocean-atmosphere system have more than one stable mode of operation? Nature 315 : 21–26

Brutsaert W (1982) Evaporation into the atmosphere. Reidel, Dordrecht

Bryan F (1986) High-latitude salinity effects and interhemispheric thermohaline circulations. Nature 323 : 301–304

Cessi P, Young WR (1992) Multiple equilibria in two-dimensional thermohaline circulation. J Fluid Mech 241 : 291–309

Charnock H (1994) Air-sea exchanges and meridional fluxes. In: Malanotte-Rizzoli P, Robinson A R (eds) Ocean processes in climate dynamics: global and Mediterranean examples. Kluwer, Dordrecht pp 1–27

Crowley TJ, North GR (1991) Paleoclimatology. Oxford University Press, New York

Dansgaard W, Johnsen SJ, Clausen HB, Dahl-Jensen D, Gundestrup NS, Hammer CU, Hvidberg CS, Steffensen JP, Sveinbjörnsdottir AE, Jouzel J, Bond G (1993) Evidence for general instability of past climate from a 250-ky ice-core record. Nature 364 : 218–220

Dewar WK, Huang RX (1995) Fluid flow in loops driven by freshwater and heat fluxes. J Fluid Mech 297 : 153–191

Dijkstra HA, Molemaker J (1997) Symmetry breaking and overturning oscillations in thermohaline driven flows. J Fluid Mech 331 : 169–198

Doedel EJ (1981) AUTO: a program for the automatic bifurcation analysis of autonomous systems. Cong Num 30 : 265–284

Douglas RG, Woodruff F (1981) Deep sea benthic foraminifera. In: Emiliani C (ed) The Sea 7. Wiley-Interscience, New York, pp 1233–1327

Frankignoul C, Hasselmann K (1977) Stochastic climate models, Part II Application to sea-surface temperature anomalies and thermocline variability. Tellus 29 : 289–305

Haney RL (1971) Surface thermal boundary condition for ocean circulation models. J Phys Ocean 1 : 241–248

Huang RX, Stommel HM (1992) Convective flow patterns in an eight-box cube driven by combined windstress, thermal and saline forcing. J Geophys Res 97: 2347–2364

Huang RX, Chou RL (1994) Parameter sensitivity study of the saline circulation. Clim Dyn 9 : 391–409

Hughes TMC, Weaver AJ (1996) Sea surface temperature-evaporation feedback and the ocean's thermohaline circulation. J Phys Ocean 26 : 644–655

Gill AE (1982) Atmosphere-Ocean Dynamics. Academic Press, New York

Guckenheimer J, Holmes P (1983) Nonlinear oscillations, dynamical systems, and bifurcation of vector fields. Springer, Berlin Heidelberg, New York, Tokyo

Källén E, Huang X-Y (1987) A simple model for large scale thermohaline convection. Dyn Atmos Oceans 11 : 153–173

Lorenz EN (1963) Deterministic non-periodic flow. J Atm Sci 20 : 130–141

Maas LRM (1994) A simple model for the three-dimensional thermally and wind-driven ocean circulation. Tellus 46 A: 671–680

Malkus WVR (1972) Non-periodic convection at high and low Prandtl number. Mem Soc R Sci Liège 6^e IV: 125–128

Marotzke J (1994) Ocean models in climate problems. In: Malanotte-Rizzoli P, Robinson AR (eds) Ocean processes in climate dynamics: global and Mediterranean examples Kluwer, Dordrecht, pp 79–109

Marotzke J, Willebrand J (1991) Multiple equilibria of the global thermohaline circulation. J Phys Ocean 21 : 1372–1385

Marotzke J, Welander P, Willebrand J (1988) Instability and multiple steady states in a meridional-plane model of the thermohaline circulation. Tellus 40 A: 162–172

McIntyre A, Ruddiman WF, Karlin K, Mix AC (1989) Surface water response of the equatorial Atlantic Ocean to orbital forcing. Paleoceanography 4 : 19–55

Mikolajewicz U, Maier-Reimer E (1990) Internal secular variability in an ocean general circulation model. Clim Dyn 4 : 145–156

Mikolajewicz U, Maier-Reimer E (1994) Mixed boundary conditions in ocean general ciculation models and their influence on the stability of the model's conveyor belt. J Geophys Res 99 : 22633–22644

Molfino B, McIntyre A (1990) Precessional forcing of nutricline dynamics in the equatorial Atlantic. Science 249 : 766–769

Mysak LA, Stocker TF, Huang F (1993) Century-scale variability in a randomly forced, two dimensional thermohaline ocean circulation model. Clim Dyn 8 : 103–116

Nakamura M, Stone PH, Marotzke J (1994) Destabilization of the thermohaline circulation by atmospheric eddy transports. J Clim 7 : 1870–1882

Oeschger H, Beer J, Siegenthaler U, Stauffer B, Dansgaard W, Langway CC (1984) Late-Glacial climate history from ice-cores. In: Climate processes and climate sensitivity. A.G.U. Geophys Mongr 29 : 299–306

Pestiaux P, Duplessy JC, Berger A (1987) Paleoclimatic variability at frequencies ranging from 10^{-4} cycle per year to 10^{-3} cycle per year-evidence for nonlinear behavior of the climate system. In: Rampino MR, Sanders JE, Newman WS, Königsson LK (eds) Climate history, periodicity, and predictability. Van Nostrand Reinhold, New York, pp 285–299

Quon C, Ghil M (1992) Multiple equilibria in thermosolutal convection due to salt-flux boundary conditions. J Fluid Mech 245 : 449–483

Quon C, Ghil M (1995) Multiple equilibria and stable oscillations in thermosolutal convection at small aspect ratio. J Fluid Mech 291 : 33–56

Ruddick B, Zhang L (1996) Qualitative behavior and nonoscillation of Stommel's thermohaline boxmodel, J Clim 9 : 2768–2777

Schmitt RW, Bogden PS, Darmon CE (1989) Evaporation minus precipitation and density fluxes for the North Atlantic. J Phys Ocean 19 : 1208–1221

Seager R, Kushnir Y, Cane MA (1995) On heat flux boundary conditions for ocean models. J Phys Ocean 25 : 3219–3230

Sinninghe Damsté JS, Köster J (1998) An euxinic southern North-Atlantic ocean during the Cenomanian/Turonian oceanic anoxic event. Earth Planet Sci Lett (in press)

Stocker TF, Mysak LA (1992) Climatic fluctuations on the century time scale: a review of high resolution proxy data and possible mechanisms. Clim Change 20: 227–250

Stommel H (1961) Thermohaline convection with two stable regimes of flow. Tellus 13 : 224–230

Thual O, McWilliams JC (1992) The catastrophe structure of thermohaline convection in a two-dimensional fluid model and a comparison with low-order box models. Geophys Astrophys Fluid Dyn 64 : 67–95

Warren BA (1983) Why is no deep water formed in the North-Pacific? J Mar Res 41 : 327–347

Weaver AJ, Sarachik ES (1991) Evidence for decadal variability in an ocean general circulation model. Atmos-Ocean 29 : 197–231

Weaver AJ, Hughes TMC (1992) Stability and variability of the thermohaline circulation and its link to climate. Trends in Physical Oceanography Council of Scientific Research Integration Research Trends Series, Trivandrum, India

Weaver AJ, Marotzke J, Cummins PF, Sarachik ES (1993) Stability and variability of the thermohaline circulation. J Phys Ocean 23 : 39–60

Welander P (1986) Thermohaline effects in the ocean circulation and related models. In: Willebrand J, Anderson DLT (eds) Large-scale transport processes in oceans and atmosphere. Reidel, Dordrecht, pp 163–200

Winton M, Sarachik ES (1993) Thermohaline oscillations induced by strong steady salinity forcing of general ocean circulation models. J Phys Ocean 23 : 1389–1410

Wolf A, Swift JB, Swinney HL, Vastano JA (1985) Determining Lyapunov exponents from a time-series. Physica D 16 : 285–317

Wright DG, Stocker TF (1991) A zonally averaged model for the thermohaline circulation. Part 1: model development and flow dynamics. J Phys Ocean 21 : 1713–1724